Density functional study of the `titanium effect' at metal-ceramic interfaces

2000 J. Phys.: Condens. Matter 12 1209

(http://iopscience.iop.org/0953-8984/12/7/306)

J. Phys.: Condens. Matter **12** (2000) 1209–1222. Printed in the UK PII: S0953-8984(00)07201-5

Density functional study of the 'titanium effect' at metal–ceramic interfaces

S Köstlmeier and C Elsässer

Max-Planck-Institut für Metallforschung, Seestraße 92, D-70174 Stuttgart, Germany

Received 26 August 1999

Abstract. A thin interlayer of an early transition metal, e.g. titanium, can enhance the bonding at a metal–ceramic interface considerably. The role of the electronic structure in this phenomenon (the 'titanium effect') is studied quantitatively by means of density functional calculations, employing norm-conserving *ab initio* pseudopotentials and a mixed basis of localized functions and plane waves. The weakly bonding model interface $Ag(100)/MgAl_2O_4(100)$ is chosen, in order to minimize the lattice mismatch and to concentrate on electronic interactions. The stepwise addition of Ti atoms at the interface from zero to one monolayer of Ti leads to a pronounced enhancement of the bonding strength ($Ag/Ti/MgAl_2O_4$). From a comparison to the more strongly bonding systems $Ag/Al/MgAl_2O_4$ with a monatomic Al interlayer and $Al/MgAl_2O_4$ it is concluded that this enhancement correlates with the reduction of the electron density in the interface layer. It is proposed that the interlayer accommodates Pauli repulsion between O anions and electron-rich Ag atoms by suitable electron redistribution, which is accompanied by pronounced energy band shifts.

1. Introduction

The adhesion at metal–ceramic interfaces can be enhanced significantly by introducing a thin layer of an early transition metal between the metal and ceramic. This phenomenon is utilized for instance in steel technology for bonding protective ceramic coatings, such as TiN or TiC, to steel surfaces with the help of Ti, Cr, or Ta interlayers [1, 2]. Another example is the application of a copper metallization layer to SiO_2 via a Cr interlayer [3], or to polycrystalline Al_2O_3 ceramic carrier materials via Ti layers when contacting microelectronic devices. The latter systems, the weakly bonding $Cu(111)/\alpha\text{-}Al_2O_3(0001)$ and the strongly adhesive $Cu/Ti/\alpha\text{-}Al_2O_3$, have been well characterized with respect to their mechanical and electrical properties, both by means of theory [4–8] and experiment [9–17]. Appropriate preparation conditions provided, the Ti interlayer in this system is non-reactive and atomically flat, as demonstrated by analytical transmission electron microscopy (ATEM) [14], high-resolution transmission electron microscopy (HRTEM) [12, 16], and elemental mapping [17]. Indications for a partial oxidation of the O ions at the interface were obtained *in situ* during the preparation [9–11] and treated semi-quantitatively later in *ex situ* ATEM investigations [14, 18]. On the other hand, earlier density functional studies of thin (0001) Ti films show a surface-specific electronic state together with core-level shifts, which may also account for the changes of the peak positions detected in the EELS experiment [19]. However, the $Cu(111)/\alpha\text{-}Al_2O_3(0001)$ interface is observed to be incoherent. Apart from the large unit cells required for thorough theoretical investigations, the lattice mismatch of this model system is a serious drawback, because it inhibits the straightforward distinction between electronic and geometric as well as elastic or plastic effects and their influence on the interface stability.

0953-8984/00/071209+14$30.00

Therefore, a metal–ceramic system with low lattice mismatch was chosen, namely M(001)/$MgAl_2O_4$(001) with M = Al or Ag. This system has been well studied recently by experimental HRTEM [20, 21] and theoretical density functional investigations [22–24]. The pure Al/$MgAl_2O_4$ interface is atomically flat and coherent with a contracted interface distance due to electron-transfer bonds between Al atoms and O ions for Al at the adhesion position on top of O. For Ag no distinct, unique translation state was determined either in theory or experiment, because only slight polarizations of the Ag film occur, and, moreover, the formation of thermodynamically more stable (111) Ag islands is monitored experimentally [20]. Therefore, the weakly bonding system Ag/$MgAl_2O_4$ is an ideal candidate for a study of interlayer effects. Preliminary results of *in situ* RHEED (reflection high-energy electron diffraction) experiments confirm that the addition of a thin Ti interlayer changes the growth mode of Ag islands to preferentially cube-on-cube [25]. Given the strong adhesion at the Al/$MgAl_2O_4$ interface, the theoretical study was extended to Al interlayers between Ag and $MgAl_2O_4$, in particular because thin Al films have been used successfully to bond ceramic systems such as TaN to α-Al_2O_3, as well [26].

On the basis of these and other previous studies on non-reactive and reactive wetting at heterophase boundaries, the following extremal cases for the enhanced interaction in the metal/interlayer/ceramic systems Ag/M/$MgAl_2O_4$, M = Ag, Ti, Al, may be considered:

(1) The 'ionic' case: partial oxidation of the interlayer with a transfer of the electron density from the metal to the ceramic.
(2) The 'covalent' case: a localized interface state where empty electronic states of Ti act as 'glue' between the electron-rich metal and the anions.
(3) The 'elastic' case: buffering of the elastic energy by smooth accommodation of the mismatch in lattice constant between the metal and ceramic.

Case (1) is inspired by the above-mentioned experimental results on reactive wetting systems [9–17]. In particular, the weakly bound electrons from Ti s states may act as electron donors to O anions whose coordination shell is disrupted by the interface. This mechanism strongly requires that the electronegativity (EN) of the interlayer element is of comparable magnitude to that of the oxide and lower than the value for the metal to be bonded. EN(Al) = 1.54 ($\approx$EN(Mg) = 1.42 according to Sanderson [27]) may be chosen as an estimate for the electronegativity of spinel, because EN(Al) is a lower bound for the electron donation capacity of the cations in spinel, which the interlayer atoms have to compete with. With EN(Ag) = 1.7 > EN(Al) = 1.54 $\approx$ EN($MgAl_2O_4$) > EN(Ti) = 1.13 this prerequisite is fulfilled to a higher degree by Ti than by Al; thus bonding should be enhanced more strongly by Ti via this mechanism.

Case (2) is based on the results of previous density functional investigations on the pure systems Al/$MgAl_2O_4$ and Ag/$MgAl_2O_4$ [22–24], where stronger adhesion was found for the free-electron-type metal Al compared to the more repulsive situation for the localized Ag d electrons and the oxide anions. A measure for this interaction may be the electron gas parameter r_s which gives the radius of a sphere containing one conduction electron of the respective element; thus the localization is weakest for the largest value of r_s. The values of r_s vary as r_s(Ag) = 0.6 Å < r_s(Ti) = 1.2 Å < r_s(Al) = 1.3 Å, which indicates that in this regime the effect of enhancement by Al should be more pronounced.

Case (3) is often discussed as an important factor having influence on the mechanical behaviour of composite and fibre-reinforced materials [28–30]. Due to the negligible lattice mismatch, this mechanism is not expected to play a role in the model system Ag/$MgAl_2O_4$. However, elastic contributions to the energy balance at the interface can arise upon exchange of Ag atoms with Ti atoms; they will be addressed below.

A short overview of (1) the computational details and (2) the composition of the supercell models is given in section 2. In section 3 the changes in the work of adhesion, W_{ad}, and the total energy, E_{tot}, are discussed as regards their dependence on (1) a stepwise addition of Ti atoms at the interface and (2) the change of the interlayer element to Al. In section 4 site-projected densities of electronic states (PDOS) are used to analyse differences between the various interlayer systems with respect to their electronic structure at the interface. From the shifts of the PDOS at the oxygen site of $MgAl_2O_4$, changes of the Schottky barrier height are derived. A detailed analysis of the electron redistributions across the interfaces is given by means of electron density and density-difference maps. This yields a pictorial representation of the modifications of the electronic structure at the interface due to the presence of a metallic interlayer.

2. Computational method

2.1. Pseudopotential band-structure calculation

Ab initio band-structure calculations were performed in the framework of the local density functional theory [31–34] to obtain self-consistent total energies, densities of electronic states, and valence electron densities [35–38]. Norm-conserving ionic pseudopotentials were generated [39] for various atomic reference configurations of O ([He] $2s^2 2p^{3.75} 3d^{0.25}$), Mg ([Ne] $3s^{1.5} 3p^{0.25} 4d^{0.25}$), Al ([Ne] $3s^2 3p^{0.75} 3d^{0.25}$), Ag ([Kr] $5s^{0.75} 5p^{0.25} 4d^{10}$), and Ti ([Ar] $4s^{0.60} 4p^{0.80} 3d^{2.60}$) and employed to represent the core–valence interactions. The valence electron Bloch states were treated in a mixed-basis formalism of plane waves ($E_{pw} = 485$ eV) and additional local orbitals for 2p states of O ($r_{lo} = 0.92$ Å), for 3d states of Ti ($r_{lo} = 1.05$ Å), and for 4d states of Ag ($r_{lo} = 1.05$ Å). The Kohn–Sham effective one-particle equations for the 11-layer supercells were solved for a $4 \times 4 \times 1$ Monkhorst–Pack k-point mesh [40].

The interface works of adhesion W_{ad} given in the following discussion were calculated in an idealized sense by subtracting the total energies of the rigid metal and oxide free-surface slabs from the total energy of the interface system. As no relaxations of the free metal or oxide surfaces were considered, the calculated values of W_{ad} are upper bounds for the actual work of adhesion W_{ad}^0. Therefore, the changes to W_{ad} are used merely for a qualitative analysis of trends.

Densities of valence electron states were analysed locally by projection in spheres at the atomic sites (PDOS). The projection radii were adjusted to yield touching spheres for metallic Al and Ag, as well as for the oxygen anions. The spheres for the cations Mg and Al in spinel were chosen to fit into the interstitial sites of the distorted face-centred-cubic sublattice of the oxygen anions. The PDOS curves were convoluted with a Gaussian of 0.5 eV broadening width for facilitating the analysis of shifts and shape changes caused by interface modifications.

In order to obtain the maps of the valence electron density differences, first, the distributions of valence electron densities for the total interface system and for the individual metal and spinel slabs were calculated separately with supercells of identical size. Second, the slab densities were superposed; then this superposition was subtracted from the electron density of the interface system.

2.2. Choice of models

Ti enrichment at metal–ceramic interfaces has been observed in numerous systems with film thicknesses in the sub-monolayer–micron range [1, 41]. In the present investigation only the low-coverage regime is analysed with Ti contents of 0, 1/4, 1/2, 3/4, and 1 monolayer

(ML). The geometry of the corresponding supercell is depicted schematically in figure 1. The model systems were composed of stacked sequences of four AlO and three Mg (001) layers of spinel, a (001) metal interlayer, two Ag (001) layers, and another (001) metal interlayer, and repeated by three-dimensional periodic boundary conditions. According to previous results for the Al/$MgAl_2O_4$ system the oxide was terminated by dense-packed Al/O layers, and a lateral translation state with the interlayer metal atoms on top of the spinel O ions was assumed [21, 23, 24]. The axial component of the translation state between the oxide and the interlayer was optimized for the presence of a Ti monolayer as 1.99 Å, whereas a fixed distance of 1/4 of a_0 within the slabs was chosen, where a_0 is the calculated lattice constant of bulk spinel (calculated: 8.007 Å [22]; experimental: 8.088 Å [42]). An undisturbed continuation of the fcc lattice was chosen between the interlayer and the two-layer Ag slab.

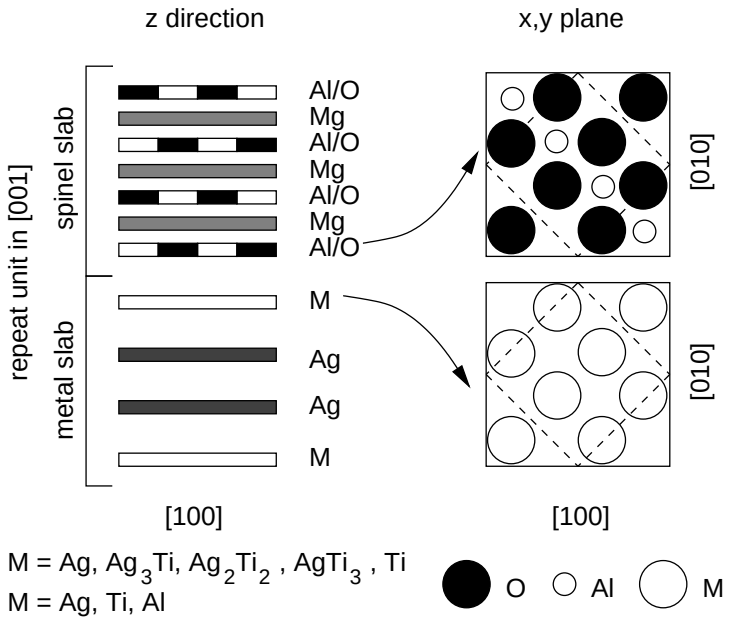

Figure 1. A schematic representation of the supercell models employed for the present study. Displayed are the stacking sequence of spinel and metal planes along the [001] direction and the cube-on-cube orientation of the interface (x, y) planes. The dashed lines on the (x, y) planes mark the lateral supercell size.

Two further supercells were investigated: one system with complete Al monolayers between the spinel and Ag, and another one with a full four-layer Al slab. For the present analysis of the electronic structure all geometric parameters of these model systems were chosen identical with the ones described above. In the discussion of the adhesion energetics (section 3.2) comparison is also made to the relaxed structures with interface distances of $d_{int} = 1.90$ Å (Al/$MgAl_2O_4$) and $d_{int} = 2.35$ Å (Ag/$MgAl_2O_4$) calculated previously [23, 24].

3. Adhesion energetics

3.1. Variation of the Ti content

The schematic representation of the supercells in figure 1 displays eight atoms at the interface unit, which corresponds to twice the unit cell in the (x, y) plane used in the calculation.

Therefore, the variation between 0, 1/4, 1/2, 3/4, and 1 ML of Ti at the interface can be achieved by successive exchange of all four metal atoms per interface unit. The corresponding models are denoted as Ag/Sp (=Ag/Ti_0/Sp), Ag/Ti/Sp (=Ag/Ti_1/Sp), and Ag/Ti_n/Sp, where $n = 1/4$, 1/2, and 3/4, and Sp stands for spinel. In the case of half a monolayer, two different arrangements of the two Ti and the two Ag atoms at the interface were considered: the nearest-neighbour arrangement where atoms of the same element were aligned parallel to the ⟨110⟩ directions of the substrate, and the next-nearest-neighbour arrangement with the alignment along ⟨100⟩ directions.

From the calculations for the systems Ag/Sp and Ag/Ti/Sp the change of the total energy $\Delta_{slab}E_{tot}$ was obtained for the exchange of the complete interlayer metal slab from Ag to Ti. Division by four gives the average change of E_{tot} per Ag → Ti atom exchange, $\overline{\Delta_{slab}E_{tot}}$. By subtracting $\overline{\Delta_{slab}E_{tot}}$ from the successive changes $\Delta_n E_{tot}$ per atom exchange, one obtains the quantity listed in columns 2 and 3 of table 1 separately for the two different atom arrangements of (Ag/$Ti_{1/2}$/Sp). Negative values indicate that the corresponding Ag → Ti exchange step is energetically more favourable than the exchange of the whole monolayer; positive values signify the opposite.

Table 1. Changes of the total energy, $\Delta E_{tot} = \Delta_n E_{tot} - \overline{\Delta_{slab}E_{tot}}$ (see the text, section 3.1), and the work of adhesion, ΔW_{ad}, upon successive exchange for Ag atoms of Ti atoms at the interface layer (in J m^{-2}). The Ti atoms of the half-monolayer are arranged along ⟨100⟩ directions for the values in columns 2 and 4, and along ⟨110⟩ for columns 3 and 5. Columns 2 and 3 give deviations from the average change of E_{tot}, $\overline{\Delta_{slab}E_{tot}}$, for the stepwise Ag → Ti atom exchange; columns 4 and 5 give the absolute contribution from each Ti atom to W_{ad} from a comparison to the energies of the free four-layer slabs, Ag–Ag–Ag–Ag and Ti–Ag–Ag–Ti.

	ΔE_{tot}		ΔW_{ad}	
System	⟨100⟩	⟨110⟩	⟨100⟩	⟨110⟩
1/4 ML	−0.04	−0.04	+0.54	+0.54
1/2 ML	−0.39	+2.78	+0.89	−2.49
3/4 ML	+0.32	−2.85	+0.12	+3.50
1 ML	+0.11	+0.11	+0.36	+0.36
Total	0.0	0.0	+1.91	+1.91

For the ⟨100⟩ atom arrangement of (Ag/$Ti_{1/2}$/Sp) the first two exchange steps enhance the bonding more strongly than the third and fourth step; therefore the strongest bonding per Ti atom at the interface is obtained for half a monolayer. The values of the change in E_{tot} are considerably higher for the ⟨110⟩ arrangement of (Ag/$Ti_{1/2}$/Sp); in this case the second Ag → Ti step is already energetically strongly disfavoured, where nearest neighbours of Ti are formed. This effect may be related to an additional elastic contribution in the interlayer upon Ti addition (case (3)), because the equilibrium distances d(Ti–Ti) of pure hcp Ti and hypothetical fcc Ti were calculated to give 2.86 Å (experimental: 2.95 Å; c/a ratio: calculated: 1.61, experimental: 1.59) and 2.82 Å, respectively, and thus they are slightly larger than the nearest-neighbour distance d(Ag–Ag) = d(O–O) = 2.81 Å at the interface.

For an estimate of the elastic energy, the B1 (rock-salt) and B2 (caesium chloride) polymorphs of the hypothetical bulk binary intermetallic compound AgTi were investigated, where the atoms of the same element are aligned in the ⟨100⟩ direction in the B1 structure and in the ⟨110⟩ direction in B2. At their respective equilibrium lattice constants, the B2 structure is more stable than B1 by 0.11 J/(AgTi unit). The equilibrium distances amount to: d(Ag–Ti) = 3.23 Å (B1) and 2.78 Å (B2), and d(Ag–Ag) = d(Ti–Ti) = 3.73 Å (B1) and 3.24 Å (B2). In figure 2 E_{tot} is plotted as function of d(Ti–Ti) for both polymorphs, because

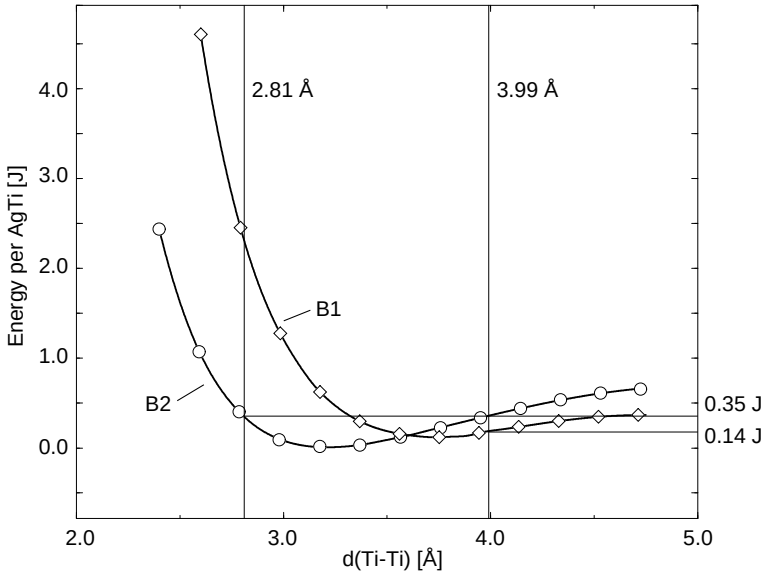

Figure 2. Total energy (in eV) of the B1 and B2 polymorphs of TiAg versus the shortest distance between two Ti atoms, d(Ti–Ti) (in Å), upon isotropic expansion of the cell volume. The vertical lines indicate the two shortest possible Ti–Ti distances in the interlayer of the Ag/Ti/Sp system. The lowest energy is obtained for the B1 structure with the next-nearest-neighbour arrangement of Ti at d(Ti–Ti) = 3.73 Å with a value of d(Ag–Ti) = 3.23 Å.

d(Ti–Ti) is the geometrical parameter determining the elastic contribution due to the lattice mismatch between Ti and Ag or spinel. Vertical lines denote the two possible values of d(Ti–Ti) in the interlayer: the nearest-neighbour distance of 2.81 Å with an alignment of Ti atoms along ⟨110⟩ as in the B2 structure and the next-nearest-neighbour distance of 3.99 Å with an alignment along ⟨100⟩ as in the B1 structure. Under the geometric constraints given at the interlayer, the lower total energy is obtained for the B1 structure with a next-nearest-neighbour arrangement of the Ti atoms and an elastic contribution of 0.14 J/(AgTi unit) compared to the equilibrium structure. For the B2 structure the corresponding elastic contribution amounts to a higher value of 0.35 J/(AgTi unit). This is concomitant with the finding that the ⟨100⟩ atom arrangement shows the more favourable energy balance. Although these values were derived for the bulk AgTi crystals, they can be considered as upper bounds for the actual elastic interaction. It may thus be concluded that compressive stresses are acting on the Ti interlayer, starting from a coverage of half a monolayer in the ideal case.

Instead of the bulk crystals, reference can be made also to the difference in total energies of the two free four-layer surface slabs Ag–Ag–Ag–Ag and Ti–Ag–Ag–Ti. From this analysis one obtains a noticeable increase of the work of adhesion by 1.91 J m^{-2} when a complete Ti interlayer is introduced. Using this value the contribution of each Ag $\rightarrow$ Ti exchange to the change of W_{ad}, ΔW_{ad}, can be calculated from columns 2 and 3 in table 1. The corresponding data are listed in columns 4 and 5, and show trends similar to those in the above discussion of the total-energy change. Again, the major part of the bonding enhancement is given by half a monolayer of Ti in the ⟨100⟩ arrangement, whereas the third and fourth step account for only about one quarter to one fifth of the interaction. Yet all steps are accompanied by an increase of W_{ad}. In contrast, for the ⟨110⟩ arrangement the repulsion of the directly neighbouring Ti atoms prevails, so the second exchange step is highly energy intensive.

3.2. Variation of the interlayer element

Absolute values of the ideal work of adhesion are obtained by referencing to the total energy of the unrelaxed free surfaces of both the metal and spinel slabs (cf. table 2). The additional bonding contribution of 1.91 J m^{-2} upon exchange of the full Ag interface layer for Ti atoms increases W_{ad} of Ag/Sp at $d_{int} = 1.99$ Å from the non-bonding situation with -0.10 J m^{-2} to 1.81 J m^{-2} in Ag/Ti/Sp. At the optimized value of the interface distance for Ag/Sp, $d_{int} = 2.36$ Å, W_{ad} of Ag/Sp was calculated as 1.10 J m^{-2}; thus the net adhesion enhancement for Ag on spinel by the Ti interlayer amounts to 0.71 J m^{-2} and a contraction at the interface by 0.37 Å.

Table 2. Ideal work of adhesion in the following systems: Ag/Sp, Ag/Ti/Sp, Ag/Al/Sp, and Al/Sp at the optimized interface distance, $d_{int} = 1.99$ Å, of the system Ag/Ti/Sp (in J m^{-2}). A double vertical line || denotes the cleavage plane. The values in parentheses give the values of W_{ad} at the optimized interface geometries for Ag/Sp ($d_{int} = 2.35$ Å) and Al/Sp ($d_{int} = 1.90$ Å).

Cleavage plane	Ag/Ag	Ag/Ti	Ag/Al	Al/Al
M/M′||Sp	−0.10	1.81	2.94	1.99
	(1.10)	(1.81)	—	(2.25)
M||M′/Sp	—	5.94	5.39	—
M||M′	—	6.52	8.85	—
M′||Sp	—	2.38	3.04	—

For the strongly bonding system Al/Sp a value of 2.25 J m^{-2} had been calculated previously at an optimized $d_{int} = 1.90$ Å [22–24], whereas $W_{ad} = 1.99$ J m^{-2} at $d_{int} = 1.99$ Å, in rather close agreement with the result for the Ag/Ti/Sp system. Comparing these values, it is concluded that the Ti interlayer changes the adhesion between Ag and spinel from non-bonding to bonding ('non-wetting to wetting'). However, the bonding is still weaker than in the related two-component interface Al/Sp. Therefore, additional calculations were carried out for a system where a layer of Al was inserted instead of the Ti interlayer at a fixed value of $d_{int} = 1.99$ Å. For this model system, denoted as Ag/Al/Sp, a value of $W_{ad} = 2.94$ J m^{-2} was obtained, which yields a net adhesion enhancement for Ag on spinel by 1.84 J m^{-2} after subtraction of the optimized W_{ad}(Ag/Sp) $= 1.10$ J m^{-2}. Compared to those in the system Ag/Ti/Sp, the interactions in the Ag/Al/Sp system lead to an even stronger net adhesion enhancement for Ag on spinel by the Al interlayer. This effect may be related to the fact that the lattice mismatch between Al and $MgAl_2O_4$ is negligible and hence no compressive stresses act on an Al interlayer, adding a weakening elastic contribution.

For completeness, the energies for an ideal cleavage at the interface between Ag and the interlayer element are given in table 2 together with the works of adhesion within the corresponding slabs. Since all values are higher compared to W_{ad} at the metal–ceramic interface, this failure mechanism was not considered further in the following.

4. Changes in the electronic structure

4.1. Projected densities of states

Further insight into the different modes of interaction between the three metals—Al, Ti, and Ag—and the spinel surface can be obtained from projected densities of states (PDOS) within spheres around atomic sites. A direct comparison of the three metals is complicated by the pronounced differences which arise already for the electronic structures of the corresponding bulk crystals, Al being a main-group metal, and Ti an early and Ag a late transition metal.

Consequently, the PDOS of the pure metals already differ considerably in shape. A better choice for a comparison are the PDOS for the O sites of the spinel slab, as the only differences between them occur due to the response of the O anions to the presence of the respective metal. In the interface models studied here, there exist four different O positions, which are not equivalent by symmetry: two of the positions are located in the interface layer; the other two sites belong to the Al/O layer in the interior of the oxide film.

Figure 3 gives an overview of the changes to the O-PDOS at the interface and interior (interface $-$ 1) layers computed for the systems Ag/Sp, Ag/Ti/Sp, Ag/Al/Sp, and Al/Sp, in which the whole (001) interlayers are exchanged. The optimized value of $d_{int} = 1.99$ Å was chosen in all cases in order to exclude additional changes of the splitting due to different crystal-field effects. As discussed previously for the free spinel slab, the O-PDOS of the interior layer is shifted by -0.4 eV to higher binding energies compared to the O-PDOS of pure spinel. This effect is caused by an Mg understoichiometry of the present model systems. The extensive study of various model sizes [24] has demonstrated that this effect is negligible as regards the discussion of the adhesion at the metal–spinel interface. For the weakly bonding Ag/Sp system at equilibrium, interface distance shifts of about -2 eV were calculated; hence the additional shifts of the interior O-PDOS s and p levels reflect the change of the chemical potential upon reaction with the interlayer metal.

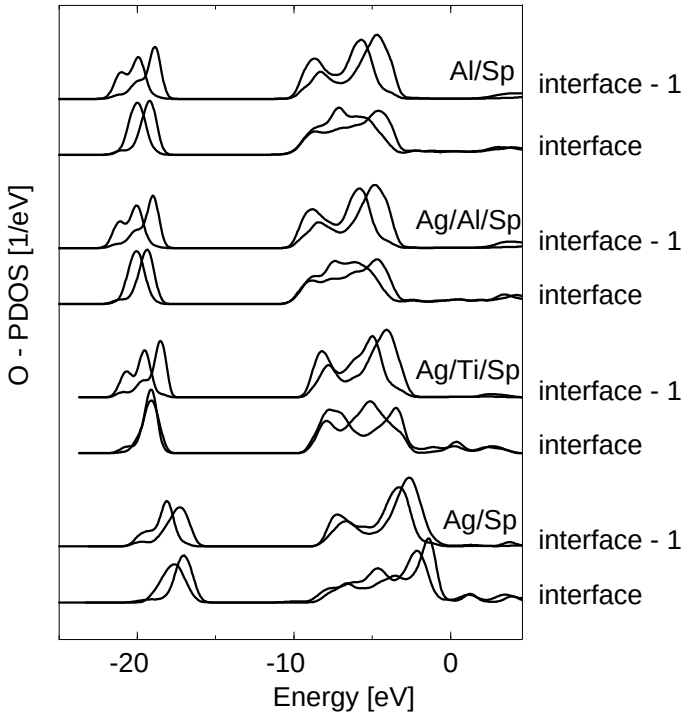

Figure 3. PDOS curves projected on the O site of the interface model systems Al/Sp, Ag/Al/Sp, Ag/Ti/Sp, and Ag/Sp (from the top). The O sites directly located at the interface are denoted by 'interface'; the O sites in the interior of the spinel slab are termed 'interface $-$ 1'.

In addition to this effect, the O anions at the interface exhibit further splittings due to the direct bonding interaction with the metal atom which is adsorbed directly above it. For the pure system Ag/Sp, it can be concluded that the interaction across the interface is strong,

because the splitting of the 2p bands of the O anions at the interface is considerably enhanced compared to the other three cases. Yet, considering the energy balance given in section 3.2, this interaction is repulsive at $d_{int} = 1.99$ Å.

In the Ag/Ti/Sp system, the onsets of the O-PDOS curves of the first-layer oxide ions are shifted more strongly than in the case of Ag/Sp. Also the curves' shapes differ significantly (cf. figure 3) from the weakly bonding case of Ag/Sp. For the O ions at the interface, a shift by about -4 eV is obtained along with a decrease of the splitting that is already reminiscent of the Al/Sp model. For the second type of interlayer, Al in Ag/Al/Sp, a similar picture is observed: compared to the bulk-like O-PDOS of the interior layer, the O anions directly at the interface display slight modifications of the PDOS, which resemble more closely the situation of the Al metal atoms in the corresponding Al/Sp system than that in the Ag/Ti/Sp system.

For a better comparison of the O-PDOS of both Al/Sp and Ag/Al/Sp, figure 4 shows the overlay of site-resolved PDOS curves calculated for the Al/Sp (solid line) and Ag/Al/Sp (dotted line) systems, both for all oxygen anions and for all Al atoms. In the spinel film especially, the site-resolved PDOS curves are virtually identical. This is another indication that the interactions at this metal–ceramic interface are rather close to those of the pure interface system Al/Sp with only minor differences. Also displayed are the PDOS of the Al metal layers. There, the differences between the two systems are again small compared to the differences between the two non-unique adhesion sites at each interface, which reflect the shape of the corresponding O bonding partner on the spinel side of the interface. The last curve shows the PDOS of the interior Al layer of the Al/Sp system and has an almost bulk-like shape. These observations confirm that the metal–ceramic interaction is confined to the layers directly

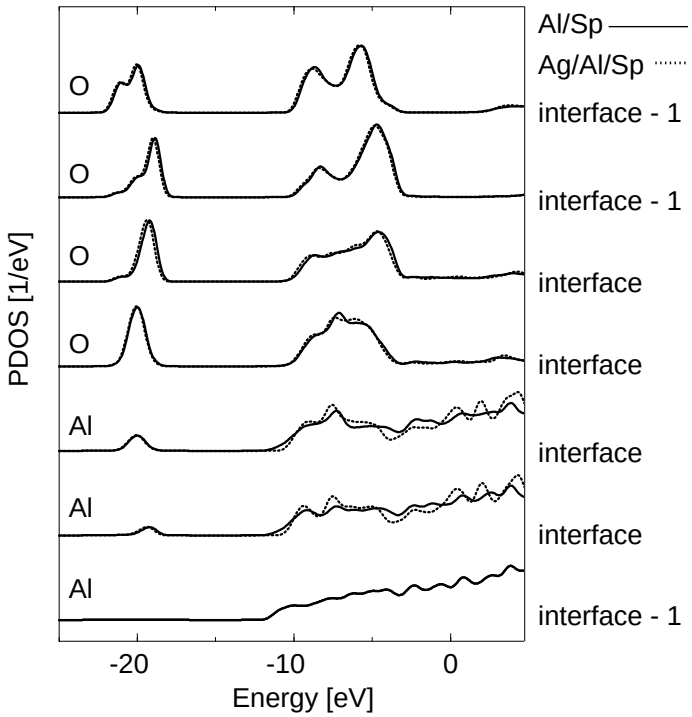

Figure 4. PDOS curves projected on spinel O sites and metal Al sites of the model systems Al/Sp (solid line) and Ag/Al/Sp (dotted line) in a site-resolved comparison.

adjacent to the interface and that this characteristic is not altered by the presence of an additional metallic interlayer.

From the energy shifts of the O-PDOS, the height of the Schottky barrier Φ_S can be estimated by subtraction from the experimental band-gap energy $E_G = 7.8$ eV [43] of spinel. Figure 5 displays the changes to the Schottky barrier when the constitution at the interface is changed. Concomitant with the modifications of the O-PDOS discussed above, the values of Φ_S decrease in the following order: $\Phi_S(\mathrm{Ag/Sp}) = 5.1\ \mathrm{eV} \gg \Phi_S(\mathrm{Ag/Ti/Sp}) = 3.7\ \mathrm{eV} > \Phi_S(\mathrm{Ag/Al/Sp}) = \Phi_S(\mathrm{Al/Sp}) = 3.3\ \mathrm{eV}$. Additionally one can evaluate Φ_S for the systems in which the interlayer constitution is changed in a stepwise fashion. All values are within the range spanned by the systems Ag/Sp and Al/Sp, and a decrease of Φ_S is obtained with increasing Ti content as follows: $\Phi_S(\mathrm{Ag/Ti_{1/4}/Sp}) = 4.6\ \mathrm{eV} \approx \Phi_S(\mathrm{Ag/Ti_{1/2}/Sp}) = 4.5\ \mathrm{eV} > \Phi_S(\mathrm{Ag/Ti_{3/4}/Sp}) = \Phi_S(\mathrm{Ag/Ti_1/Sp}) = 3.7\ \mathrm{eV}$. For this comparison only the energetically favoured ⟨100⟩ arrangement of Ti and Ag atoms was chosen. These results may be an indication that the Schottky barrier height does not correlate linearly with the excess of Ti at the interface, but that the barrier is influenced as well by the elastic interactions discussed already for the enhancement of the work of adhesion.

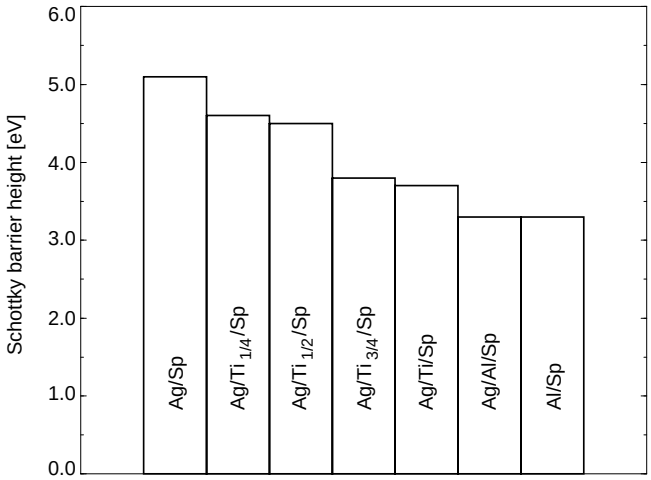

Figure 5. Schottky barriers (in eV) calculated by subtracting the shifts of the O p bands of the seven model systems from the experimental value of the spinel band gap, 7.8 eV.

4.2. Electron density distribution

Following the discussion of the elastic contribution (case (3) in section 1), a differentiation between the ionic case (1) and the covalent case (2) is attempted by means of an analysis of the spatial electron distribution for the different interlayer systems. In figure 6 the valence electron density is integrated over planes parallel to the interface and displayed as a function of the direction perpendicular to the interface for the systems Ag/Sp, Ag/Ti/Sp, Ag/Al/Sp, and an overlay of the three curves (from top to bottom). No pronounced changes occur for the interior layers of spinel, and also the changes to the interior Ag layers of the metal slab are very small. The main differences occur for the interface layer, where a pronounced maximum is found for the pure Ag film, which tends to spill out slightly towards the spinel, and the peak of the spinel interface layer is modified in comparison to the slab interior. For M = Ti the electron density at the interlayer is reduced considerably; thus the spinel electron density can decrease to its minimum value at the Mg layers and additionally spill out slightly towards the metal slab. For M = Al the same trends are observed as for Ti, the only difference being the

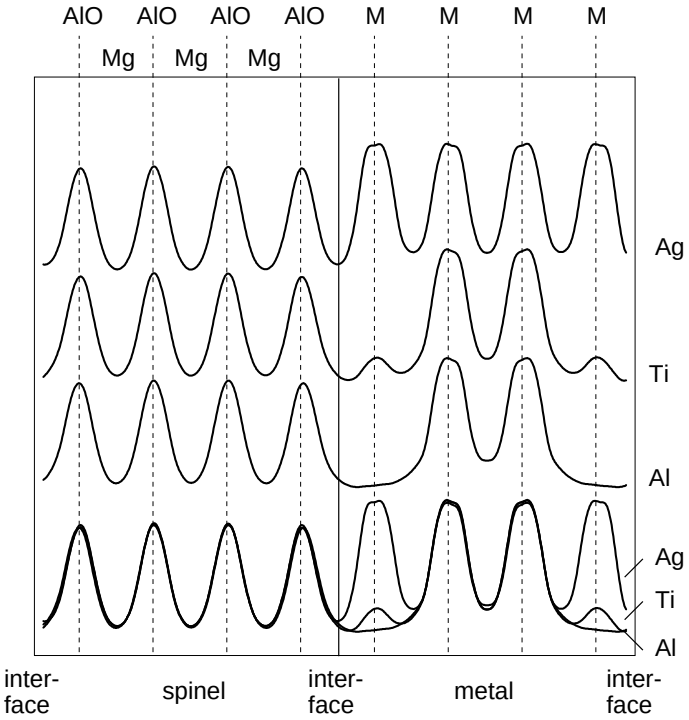

Figure 6. Electron density integrated over planes parallel to the interface for the model Ag/Sp, Ag/Ti/Sp, AgAl/Sp, and a superposition of the three curves (from the top). Vertical lines indicate the positions of the dense-packed AlO(001) planes of the spinel slab and the (001) planes of the metal slab.

even lower electron density at the interface. From this integrated quantity no indications for an oxidation of the interlayer metal can be deduced; hence the covalent case (2) more probably provides the dominant interaction.

A confirmation of this result can be obtained from the electron density and density-difference maps depicted in figure 7 and figure 8 for the systems Ag/Sp, Ag/Ti/Sp, and Ag/Al/Sp. The plots show cuts perpendicular to the interface with the interface intersecting the cut plane at 1/8, 3/8, 5/8, and 7/8 of the [001] direction. White spots of the electron density distributions in figure 7 denote areas of high density, such as the d electrons of Ag and the p electrons of the spinel oxide anions, and dark contours signify areas of low density. As for the integrated electron densities (figure 6), no major differences occur at the interior spinel layers, where the O positions show up as bright spots and the pronounced dark features correspond to the valence electron-poor environment of the Mg cations. The interior layers of the metal slabs behave in a similar fashion: the densities of the Ag layers of Ag/Ti/Sp and Ag/Al/Sp do not differ significantly from the situation in Ag/Sp. At the interface, however, a stepwise electron depletion is clearly discernible in the order Ag/Sp > Ag/Ti/Sp > Ag/Al/Sp.

The finding of an electron depletion layer does not allow the distinction between ionic case (1) and covalent case (2), because it does not include information about the electron transfer at the interface. For this purpose the electron density-difference maps of figure 7 were calculated, where bright contours depict areas of electron enrichment and dark ones electron depletion, referred to the free metal and spinel slabs. In the system Ag/Sp the close vicinity of spinel and Ag slabs induces a considerable charge redistribution within the Ag slab, whereas the fixed ion

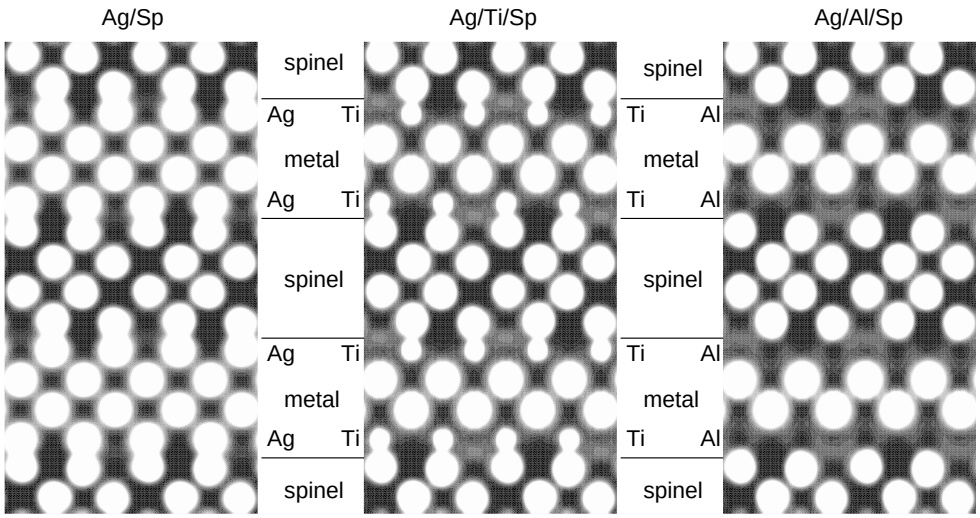

Figure 7. The electron density distribution in a plane intersecting the O and Al sites of the spinel and M atoms of the metal slab for the models Ag/Sp, Ag/Ti/Sp, and Ag/Al/Sp (from the left). Bright contours indicate local maxima of the valence electron density, dark contours areas of low electron density. The line spacing is 0.005 electrons Bohr^{-3} (1 Bohr $\approx$ 0.529 Å), corresponding to steps of 1% of the maximum valence electron density of Al/Sp in this plane.

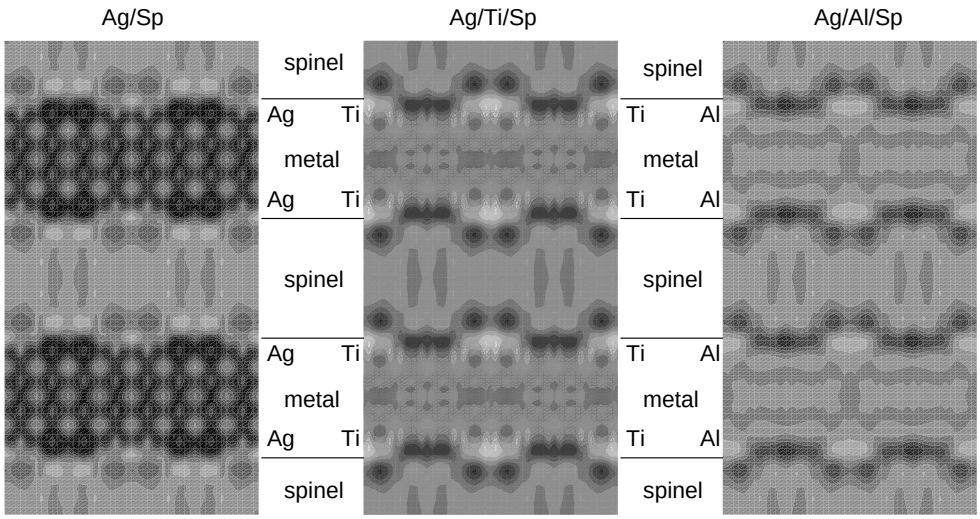

Figure 8. The electron density difference in a plane intersecting the Mg sites of the spinel for the models Ag/Sp, Ag/Ti/Sp, and Ag/Al/Sp (from the left). Bright contours indicate electron accumulations, dark contours areas of electron depletion. The line spacing is 0.001 electrons Bohr^{-3}.

arrangement of spinel is not subject to pronounced changes. Moreover, the contours within the spinel slab remain virtually the same regardless of the system considered, and the only differences that occur are very localized at the interface.

Compared to Ag/Sp, the systems Ag/Ti/Sp and Ag/Al/Sp exhibit very similar features: the metal–ceramic interaction is already well screened after the first metal layer, i.e. by the metallic

interlayer, especially in the case of M = Ti. The electron redistribution is restricted mainly to the layers at the interface, and exhibits a complex pattern of electron transfer from and to the metal interlayer. As a slight difference between the two interlayer metals, the redistribution pattern is more localized in the case of M = Ti. These electron accumulations may arise from the fact that Ti is under compressive stress in the interlayer and the electrons have to screen the interaction between neighbouring Ti cores. Altogether, there is no flat, continuous depletion contour in the interlayer metal which would signify a partial oxidation; thus the covalent interaction (2) dominates over the ionic contribution (1) in both systems, Al and Ti.

5. Conclusions

Ab initio band-structure calculations were performed in the framework of the local density functional theory, with norm-conserving ionic pseudopotentials and a mixed basis, to study the enhancement of metal–ceramic adhesion by thin metal interlayers. Monolayers of Ti and Al were introduced into the weakly bonding interface system Ag(100)/$MgAl_2O_4$(100). This model system was selected as a good candidate for elucidating the role of the electronic structure concerning the enhancement phenomenon because of the low lattice mismatch between Ag and spinel. Three possible contributions to the enhancement are discussed: (1) partial oxidation of the interlayer upon reactive wetting, (2) covalent bonding with electron accommodation by hybridization, and (3) buffering of elastic stresses.

An analysis of the energy changes upon stepwise exchange of Ag atoms for Ti at the interface shows the influence of elastic contributions on the adhesion. In fact, for the Ti interlayer the lattice mismatch between Ag and Ti is counter-productive and the interlayer is subjected to compressive stress from half-a-monolayer coverage on. This bias in elastic energy reduces the net enhancement to a total value of 0.71 J m^{-2}, but does not counteract it. On the contrary, for an Al interlayer no unfavourable elastic interaction occurs, and the adhesion enhancement by the Al interlayer amounts to 1.84 J m^{-2}.

An analysis of projected densities of states (PDOS) at the O sites of the spinel slab underlines this trend. Major shifts to higher binding energies are obtained for the interface systems with a metallic interlayer compared to the pure Ag/Sp system. This leads to a non-linear decrease of the Schottky barrier with increasing excess of Ti at the interface. For M = Al the PDOS curves were compared to a reference system with a pure four-layer Al slab: the striking similarity of the features both at the O sites and the metal Al sites indicates that the adhesion is due to direct Al–O bonds across the interface, as discussed previously in reference [23].

This picture is confirmed by an analysis of electron density and density-difference plots: the interaction is confined to the layers directly located at the interface, whereas the interior of the spinel and Ag layers do not participate significantly. An electron depletion layer is introduced by the interlayer element unlike in the adhesion of the pure Ag film on the spinel, thus screening the unfavourable interaction of the charge accumulations localized at the Ag and the O sites. From the complicated pattern of the electron redistribution between the interlayer metal and the spinel O atoms, it is concluded that the adhesion enhancement at the interface is assisted by directed metal–oxygen bonding, whereas no considerable ionic contribution is detected.

Acknowledgments

This work was supported by the Volkswagen Stiftung, through project No VW I/70502, and by the Deutsche Forschungsgemeinschaft through project No EL155/7-1. The authors are

grateful for the good collaboration with T Wagner (MBE preparation of thin-film samples), R Schweinfest and F Ernst (HRTEM investigations). They acknowledge many stimulating discussions with M W Finnis, A T Paxton, and T Ochs.

References

[1] Kim S B, In C B, Choi S K and Chun S S 1991 *J. Physique* IV **1** 609
[2] Andrieux M *et al* 1998 *Ann. Chim.-Sci. Mater.* **23** 301
[3] Bischof J, Scherer D, Herminghaus S and Leiderer P 1996 *Phys. Rev. Lett.* **77** 1536
[4] Kasowski R V, Ohuchi F S and French R H 1988 *Physica* B **150** 44
[5] Johnson K H and Pepper S V 1982 *J. Appl. Phys.* **53** 6634
[6] Zhao G L, Smith J R, Raynolds J and Srolovitz D J 1997 *Interface Sci.* **3** 289
[7] Nath K and Anderson A B 1989 *Phys. Rev.* B **39** 1013
[8] Alemany P, Boorse R S, Burlitch J M and Hoffmann R 1993 *J. Phys. Chem.* **97** 8464
[9] Gautier M, Pham-Van L and Durand J P 1992 *Europhys. Lett.* **18** 175
[10] Guo Q and Møller P J 1991 *Surf. Sci.* **244** 228
[11] Møller P J and Guo Q 1991 *Thin Solid Films* **201** 267
[12] Dehm G 1995 *Dissertation* Universität Stuttgart
[13] Scheu C 1995 *Dissertation* Universität Stuttgart
[14] Scheu C, Dehm G, Müllejans H, Brydson R and Rühle M 1995 *Microsc. Microanal. Microstruct.* **6** 19
[15] Dehm G, Scheu C, Möbus G, Brydson R and Rühle M 1997 *Ultramicroscopy* **67** 207
[16] Bernath S 1997 *Dissertation* Universität Stuttgart
[17] Plitzko J 1998 *Dissertation* Universität Stuttgart
[18] Scheu C, Dehm G, Rühle M and Brydson R 1998 *Phil. Mag.* A **78** 439
[19] Feibelman P J, Appelbaum J A and Hamann D R 1979 *Phys. Rev.* B **20** 1433
[20] Schweinfest R 1995 *Dissertation* Universität Stuttgart
[21] Schweinfest R, Ernst F, Wagner T and Rühle M 1999 *J. Microsc.* **194** 142
[22] Köstlmeier S, Elsässer C, Meyer B and Finnis M W 1998 *Phys. Status Solidi* a **166** 417
[23] Köstlmeier S, Elsässer C, Meyer B and Finnis M W 1998 *Mater. Res. Symp. Proc.* **492** 97
[24] Köstlmeier S and Elsässer C 2000 *Interface Sci.* at press
[25] Polli A D, Wagner T, Gemming T and Rühle M 2000 *Surf. Sci.* at press
[26] Bahr D F, Hoehn J W, Moody N R and Gerberich W W 1997 *Acta Mater.* **45** 5163
[27] Sanderson R T 1952 *J. Chem. Educ.* **29** 539
Sanderson R T 1954 *J. Chem. Educ.* **31** 2
[28] Bassani J L, Vitek V and Alber I 1992 *Acta Metall. Mater.* **40** S307
[29] Pukanszky B and Fekete E 1999 *Adv. Polym. Sci.* **139** 109
[30] Frisch A, Kaysser W A, Zhang W and Petzow G 1992 *Acta Metall. Mater.* **40** S361
[31] Hohenberg P and Kohn W 1964 *Phys. Rev.* **136** B864
[32] Kohn W and Sham L J 1965 *Phys. Rev.* **140** A1133
[33] Ceperley D M and Alder B J 1980 *Phys. Rev. Lett.* **45** 566
[34] Perdew J P and Zunger A 1981 *Phys. Rev.* B **23** 5048
[35] Louie S G, Ho K M and Cohen M L 1979 *Phys. Rev.* B **19** 1974
[36] Elsässer C *et al* 1990 *J. Phys.: Condens. Matter* **2** 4371
[37] Ho K M, Elsässer C, Chan C T and Fähnle M 1992 *J. Phys.: Condens. Matter* **4** 5189
[38] Meyer B, Elsässer C and Fähnle M *Fortran 90 Program for Mixed-Basis Pseudopotential Calculations for Crystals* Max-Planck-Institut für Metallforschung, Stuttgart (unpublished)
[39] Vanderbilt D 1985 *Phys. Rev.* B **32** 8412
[40] Monkhorst H and Pack J D 1978 *Phys. Rev.* B **8** 5747
[41] Derby B, Xiao P and Webster J 1998 *Physica* **298** 304
[42] Zorina N G and Kvitka S S 1969 *Kristallografiya* **13** 599
[43] Bortz M L, French R H, Jones D J, Kasowski R V and Ohuchi F S 1990 *Phys. Scr.* **41** 4404